The Journal of Infectious Diseases

MAJOR ARTICLE

Genetically Diverse *Mycobacterium tuberculosis* Isolates Manipulate Inflammasome and Interleukin 1β Secretion Independently of Macrophage Metabolic Rewiring

Ana Isabel Fernandes,[1,2] Alexandre Jorge Pinto,[1] Diogo Silvério,[1,2,a] Ulrike Zedler,[3] Carolina Ferreira,[4,5] Iola F. Duarte,[6] Ricardo Silvestre,[4,5] Anca Dorhoi,[3,7] and Margarida Saraiva[1,8]

[1]Instituto de Investigação e Inovação em Saúde, Universidade do Porto, Porto, Portugal; [2]Doctoral Program in Molecular and Cell Biology, Instituto de Ciências Biomédicas Abel Salazar, Universidade do Porto, Porto, Portugal; [3]Institute of Immunology, Friedrich-Loeffler-Institut, Greifswald-Insel Riems, Germany; [4]Life and Health Sciences Research Institute (ICVS), School of Medicine, University of Minho, Braga, Portugal; [5]ICVS/3B's-PT Government Associate Laboratory, Braga, Portugal; [6]CICECO-Aveiro Institute of Materials, Department of Chemistry, University of Aveiro, Aveiro, Portugal; [7]Faculty of Mathematics and Natural Sciences, University of Greifswald, Greifswald, Germany; and [8]Instituto de Biologia Molecular e Celular, University of Porto, Porto, Portugal

The diversity of *Mycobacterium tuberculosis* impacts the outcome of tuberculosis. We previously showed that *M. tuberculosis* isolates obtained from patients with severe disease induced low inflammasome activation and interleukin 1β (IL-1β) production by infected macrophages. Here we questioned whether this differential modulation of macrophages by *M. tuberculosis* isolates depended on distinct metabolic reprogramming. We found that the macrophage metabolic landscape was similar regardless of the infecting *M. tuberculosis* isolate. Paralleling single–Toll-like receptor (TLR) activated macrophages, glycolysis inhibition during infection impaired IL-1β secretion. However, departing from TLR -based models, in infected macrophages, IL-1β secretion was independent of mitochondrial metabolic changes and hypoxia-inducible factor 1α (HIF-1α). Additionally, we found an unappreciated impact of a host metabolic inhibitor on the pathogen, and show that inflammasome activation and IL-1β production by macrophages require metabolically active bacteria. Our study highlights the potential confounding effect of host metabolic inhibitors on the pathogen and uncoupling of *M. tuberculosis*-inflammasome modulation from the host metabolic reprogramming.

Keywords. *Mycobacterium tuberculosis*; immunometabolism; inflammasome; macrophage.

Lay Summary. *Mycobacterium tuberculosis* is the causative agent of tuberculosis and the top infectious killer in the world, with around 1.3 million deaths reported annually. The genetic variability of this pathogen can shape its interaction with the host and modulate disease outcomes. We previously found that *M. tuberculosis* clinical isolates from patients with severe forms of tuberculosis evade cytosolic surveillance systems in macrophages. Here, we explored whether this evasion tactic was linked to metabolic alterations in the infected macrophages. We found that different *M. tuberculosis* isolates induced similar metabolic changes in infected macrophages. Additionally, we demonstrate that both host glycolysis and pathogen's metabolism were pivotal for maximum interleukin 1β (IL-1β) production. These findings highlight the complexity of macrophage-pathogen interactions and emphasize that bacterial metabolism should be considered in metabolic studies and may be amenable to therapeutic intervention against tuberculosis.

The metabolic reprogramming of immune cells is central to the immune response [1]. There has been a growing interest in understanding metabolic reprogramming during tuberculosis, a disease that claims over 1.3 million lives annually [2]. In experimental infections, *Mycobacterium tuberculosis* shifts the lung immune cell metabolism from oxidative phosphorylation towards glycolysis [3]. Several studies also support the metabolic reprogramming of *M. tuberculosis*-infected macrophages to fuel antimicrobial responses [3–6], although this metabolic shift is not ubiquitous amongst immune cells [7]. Monocyte-derived macrophages upregulate glycolysis, and alveolar macrophages β-oxidation and fatty acid uptake [3, 8, 9]. Furthermore, recent studies suggest an impact of the pathogen's natural diversity on the metabolic rewiring of the infected cells [10, 11].

The accumulation of tricarboxylic acid (TCA) cycle intermediates, assembly of the electron transport chain (ETC) and mitochondrial reactive oxygen species (ROS) production are linked to NLRP3 activation and interleukin 1β (IL-1β) production [12–14]. Given the key role of IL-1β in host resistance to

Received 25 June 2024; editorial decision 18 November 2024; accepted 19 November 2024; published online 21 November 2024

[a]Current affiliation: ENZIfarma SA, Vila Nova de Gaia, Portugal.

Correspondence: Margarida Saraiva, PhD, Instituto de Investigacao e Inovacao em Saude, Universidade do Porto, Rua Alfredo Allen 208, 4200-135 Porto, Portugal, (margarida.saraiva@i3s.up.pt).

The Journal of Infectious Diseases® 2025;231:e671–84

https://doi.org/10.1093/infdis/jiae583

M. tuberculosis [15], the mechanisms leading to inflammasome activation, particularly NLRP3 and AIM2, in response to this pathogen have attracted much attention [16]. Several *M. tuberculosis*-encoded proteins and lipids activate the NLRP3 inflammasome, whereas *M. tuberculosis* DNA activates AIM2 [16]. Counteracting the protective role of inflammasomes, *M. tuberculosis* has developed several mechanisms to evade NLRP3 activation [16], including action of the *M. tuberculosis*-encoded serine-threonine kinase PknF [17], the serine hydrolase Hip1 [18], and of Rv3364c [19]. We previously showed that *M. tuberculosis* isolates obtained from severe tuberculosis cases evaded macrophage cytosolic surveillance systems, while those from mild tuberculosis activated the inflammasome, thus inducing high levels of IL-1β in macrophages [20]. Here, we questioned whether distinct *M. tuberculosis* isolates differentially rewired the macrophage metabolism. We show that irrespective of their ability to induce IL-1β, the *M. tuberculosis* isolates under study similarly altered the macrophage metabolic profiles. We show that maximum IL-1β production depended on the macrophage glycolytic shift and on metabolically active bacteria. However, unlike single-Toll-like receptor (TLR) agonists [21–23], *M. tuberculosis* infection uncoupled mitochondrial metabolic alterations from inflammasome activation and IL-1β secretion. Collectively, our study highlights the importance of examining metabolic/inflammatory networks using live *M. tuberculosis* and shows the potential impact of host metabolic inhibitors on the pathogen, offering new perspectives on the immunometabolic control of cytokine responses in tuberculosis.

METHODS

Animals, Reagents, and Bacterial Stocks

C57BL/6 mice (male/female, 8–12 weeks) were maintained under specific-pathogen-free conditions at Instituto de Investigação e Inovação em Saúde or Friedrich-Loeffler-Institut. Myeloid-restricted hypoxia-inducible factor (Hif)$1a^{fl/fl}$-$LysMcre^{+/+}$ (mHIF-$1\alpha^{-/-}$), C57BL/6NJ-$Acod1^{em1(IMPC)J}$/J ($IRG1^{-/-}$), and matched C57BL/6 were provided by Dr Ricardo Silvestre and Dr Agostinho Carvalho, Life and Health Sciences Research Institute, School of Medicine, University of Minho, Portugal. Experiments followed Animal Research: Reporting of *In Vivo* Experiments (ARRIVE) guidelines, complying with European Union Directive 2010/63/EU, German Animal Welfare, and Portuguese *Direção Geral de Alimentação e Veterinária* (DGAV) regulations.

All reagents and resources are listed in Supplementary Table 1.

M. tuberculosis were cultured in Middlebrook 7H9 medium with 10% oleic albumin dextrose catalase (OADC) and 0.2% glycerol, and aliquoted stocks stored at −80°C. The bacteria concentration was calculated by colony-forming units enumeration.

Bone Marrow-Derived Macrophages Generation

Mouse bone marrow cells (tibias and femurs) were plated at 0.5×10^6 cells/mL in Petri dishes in complete Dulbecco's Modified Eagle's Medium (cDMEM) with 20% L-cell conditioned medium (LCCM) or recombinant macrophage colony-stimulating factor (M-CSF), and maintained at 37°C, 5% CO_2. Fresh medium was added on day 4, and cells harvested and plated in cDMEM on day 7. For glucose-free conditions, bone marrow-derived macrophages (BMDM) were preincubated with DMEM without glucose 2 hours before infection. For extracellular acidification rate (ECAR) assays, bone marrow suspensions from cryopreserved stocks were differentiated as above.

Alveolar Macrophages and Bone Marrow Monocytes Isolation and Infection

Alveolar macrophages were obtained by flushing phosphate-buffered saline (PBS)-2% fetal bovine serum (FBS) into the trachea of euthanized mice. Bone marrow monocytes were purified using EasySep Mouse Monocyte Isolation Kit. Cells were infected in media without antibiotics (multiplicity of infection [MOI] = 2, BMDM; MOI = 1, alveolar macrophages and monocytes). Cell pellets or culture supernatants were recovered for RNA, protein analysis, or metabolomics. Supernatants were filter sterilized.

Chemical Inhibitors or Agonists

Chemical inhibitors and agonists 2-deoxy-glucose (2-DG), dimethyl malonate (DMM), mitoTEMPO, and rapamycin were added to BMDM 2 hours before infection. Except for rapamycin, inhibitors were maintained throughout the experiment. Bacteria were treated overnight with 2-DG, DMM, or Q203 and pelleted by centrifugation before infection.

mRNA Analysis

Total RNA was extracted with TripleXtractor, converted to cDNA, and subjected to real-time PCR, with SYBR Green. Target gene mRNA expression was normalized to ubiquitin. Oligonucleotide sequences are in Supplementary Table 2.

IL-1β Quantification

IL-1β was quantified using a commercially available enzyme-linked immunosorbent assay (ELISA).

High-Performance Liquid Chromatography

Glucose and lactate were quantified in culture supernatants by high-performance liquid chromatography; HyperREZ XP Carbohydrate H + 8μM. The mobile phase (0.0025 M H_2SO_4) was refiltered and degasified for 30 minutes. Analysis was conducted with running protocol (sensitivity 8): 15 minutes at a constant flux of 0.7 mL/min at 54°C. Peaks were detected in a refractive index detector (IOTA 2, Reagents). Integration was performed using Gilson Uniprot Software.

Extracellular Flux Analysis

BMDM were incubated overnight in Cell-Tak coated XFp plates, at 1×10^6 cells/mL in cDMEM. *M. tuberculosis* were cultured as above and the concentration of disaggregated clumps adjusted in cDMEM. cDMEM was replaced with XF DMEM medium 1 hour before the assay. ECAR readings were monitored with XFp extracellular flux analyzer, while glucose, oligomycin, and 2-DG were sequentially added. BMDM were fixed in 4% paraformaldehyde (PFA) overnight and stained with 4′,6-diamidino-2-phenylindole (DAPI). Images were acquired and analyzed on Cell Insight CX7 High-Content Screening. ECAR values were normalized with total cell numbers.

THP1-ASC-GFP Differentiation, Infection, and Speck Quantification

THP1-ASC-GFP cells maintained in complete Roswell Park Memorial Institute medium (RPMI) 1640 with Zeocin and penicillin-streptomycin, were differentiated with phorbol 12-myristate 13-acetate (PMA) for 24 hours, rested for 4 days without PMA, and infected (MOI = 1). For ASC specks detection, infected cells were fixed in 4% PFA and stained with PhenoVue Hoechst 33342 and HCS CellMask Deep Red. Images were acquired in Operetta CLS High-Content Analysis System (20× water, NA 1.0) and analyzed with Harmony software.

Nuclear Magnetic Resonance-Based Metabolomics

At 24 hours postinfection, supernatants were collected and cells were washed and extracted using a biphasic extraction with methanol/chloroform/water (1:1:0.7) [24]. Resulting polar extracts were dried in a SpeedVac concentrator. Collected supernatants (including cell-free medium) underwent a protein-precipitation using cold methanol. Resulting supernatants were vacuum-dried. Cell-free medium was used to assess metabolite consumption and excretion by BMDM. For nuclear magnetic resonance (NMR) analysis, dried samples were resuspended in 600 mL of deuterated PBS (100 mM, pH 7.4) containing 0.1 mM 3-(trimethylsilyl) propanoic acid (TSP-d_4), and 550 mL of each sample was transferred to 5-mm NMR tubes. Samples were analyzed in a Bruker Avance III HD 500 NMR spectrometer, at 500.13 MHz for ^{1}H observation, at 298 K, using a 5-mm TXI probe. Standard 1D ^{1}H spectra with water presaturation (pulse program "noesypr1d", Bruker library) were acquired and processed. Metabolite assignment was based on matching spectral information to reference spectra available in Chenomx (Edmonton), BBIOREFCODE-2–0–0 (Bruker Biospin), and the Human Metabolome Database [25]. Principal component analysis (PCA) was performed in MetaboAnalyst.

In Silico Study of *M. tuberculosis* SDH-1

The 3D structure of *M. tuberculosis* SDH-1 was predicted with amino acid sequences (NCBI protein database: flavoprotein subunit [NP_214762.1], iron-sulfur subunit [NP_217836.1], and membrane anchor subunit [NP_214763.1]) exported to ColabFold (https://colab.research.google.com/github/sokrypton/ColabFold/blob/main/AlphaFold2.ipynb#scrollTo=kOblAo-xetgx) [26]. Models for each domain were individually built against pdb100 templates, and the 5 best models relaxed using AMBER software. The best models were analyzed, and superpositioned with *Mycobacterium smegmatis* SDH-1 (PDB: 7D6 V) using PyMOL Molecular Graphics System. PubChem structures used: ubiquinone-1 (compound identification [CID] 4462), DMM (CID 7943), malonate (CID 9084), and succinate (CID 160419).

Statistical Analysis

Results are represented as mean ± SD or in box-and-whiskers plots (Tukey method). Data were analyzed using GraphPad Prism. Sample size (n) is in figure legends. Normality and log normality were assessed using Shapiro-Wilk or D'Agostino-Pearson tests and outliers with Grubbs test. Statistical significance was defined as $P \leq .05$.

RESULTS

Genetically Distinct *M. tuberculosis* Clinical Isolates Elicit Similar Glycolytic Reprogramming in Macrophages

In our previous study [20], we stratified the tuberculosis severity at presentation for 681 adult patients with pulmonary tuberculosis and investigated how *M. tuberculosis* isolates recovered from patients with mild, moderate, or severe tuberculosis interacted with host cells. We found that *M. tuberculosis* isolates recovered from cases with mild disease consistently induced robust IL-1β responses in macrophages across multiple donors, whereas bacteria recovered from severe tuberculosis cases did not [20]. *M. tuberculosis* isolates 4I2 (high IL-1β inducer; mild tuberculosis) and 6C4 (low IL-1β inducer; severe tuberculosis) were selected from our larger collection of isolates as prototypes of such differences (Figure 1*A*). Given the link between macrophage metabolic reprogramming and inflammasome activation [1, 23], we questioned whether these *M. tuberculosis* clinical isolates might differentially control the macrophage metabolic shift with an impact on IL-1β release.

We first evaluated whether glycolysis affected IL-1β production by BMDM infected with either clinical isolate. Glycolysis inhibition with 2-DG, a nonmetabolizable glucose analogue (Figure 1*B*), abrogated IL-1β secretion and lowered *Il1b* expression in infected BMDM (Figure 1*C*), irrespective of the *M. tuberculosis* isolate. Similar data were observed in infected BMDM cultures deprived of glucose (Figure 1*D*). BMDM infected in the presence of 2-DG or the absence of glucose also showed a significant decrease in lactate, a glycolysis by-product (Supplementary Figure 1*A*). Downstream inhibition of the pentose phosphate pathway with 6-animonicotinamide (Supplementary Figure 1*B*) did not significantly impact IL-1β secretion by infected BMDM (Supplementary Figure 1*C*).

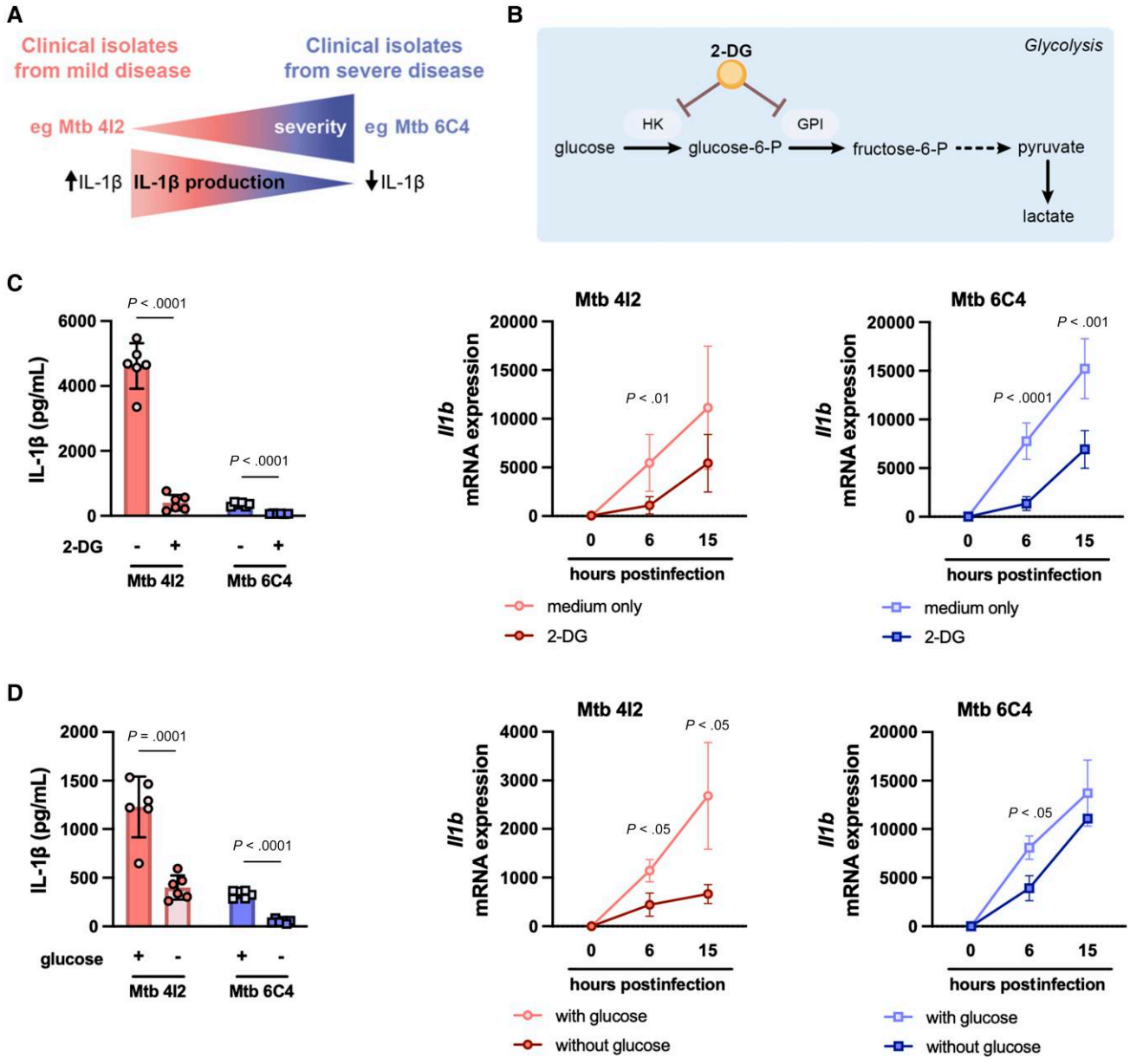

Figure 1. Glucose consumption contributes to IL-1β production by infected macrophages. *A*, Inverse correlation between disease severity and IL-1β production in cells infected with *Mycobacterium tuberculosis* 4I2 and *M. tuberculosis* 6C4, as described in Sousa et al [20]. *B*, 2-DG inhibitory action within the glycolytic pathway. *C* and *D*, Mouse BMDM were left untreated (–) or pretreated (+) for 2 hours with 2-DG (*C*) or incubated with DMEM without glucose (*D*) and subsequently infected at a multiplicity of infection of 2 with either clinical isolate. 2-DG and absence of glucose were maintained for the duration of the experiment. The amount of secreted IL-1β was quantified in the cell culture supernatants 24 hours postinfection. Six and 15 hours postinfection, cell cultures were lysed and the levels of *Il1b* determined by real-time PCR. Represented is the mean ± SD of triplicate wells for 2 experiments (*C*) or 1 experiment representative of 2 (*D*). Statistical analysis was performed using 2-tailed unpaired Student *t* test. Abbreviations: 2-DG, 2-deoxy-glucose; BMDM, bone marrow-derived macrophages; DMEM, Dulbecco's Modified Eagle's Medium; GPI, glucose-6-phosphate isomerase; HK, hexokinase; IL-1β, interleukin 1β; Mtb, *M. tuberculosis*.

Importantly, none of the inhibitors altered cell viability (Supplementary Figure 1*D*). Also, the presence of 2-DG or the absence of glucose during infection did not alter bacteria phagocytosis (Supplementary Figure 1*E*).

Given that BMDM infected with *M. tuberculosis* 4I2 or 6C4 required glycolysis to produce IL-1β, we questioned if the glycolytic shift induced by either isolate differed. Compared to noninfected cells, *M. tuberculosis*-infected BMDM showed increased glucose consumption and lactate production, with similar lactate/glucose ratios (Figure 2*A*). Consistently, gene expression for glucose transporters and glycolytic enzymes increased in both infections, with only *Slc2a1* and *Hk2* showing higher expression in *M. tuberculosis* 6C4 infections at the later time point (Figure 2*B*). ECAR assays confirmed a comparable increase in glycolysis, glycolytic

capacity, and glycolytic reserve in *M. tuberculosis* 4I2- and 6C4-infected BMDM (Figure 2*C*). Together, these data indicate a common glycolytic response to live *M. tuberculosis* infection despite downstream strain-specific differences in inflammasome activation and IL-1β production.

IL-1β Production by Infected Macrophages Is Independent of Mitochondrial ROS and mTOR

Because the differences in IL-1β secretion by *M. tuberculosis* 4I2- or 6C4-infected macrophages were not related to differential glycolysis, we investigated the contribution of other metabolic pathways. The oxidation of succinate, a TCA intermediate that accumulates in bacterial infections [27, 28], can lead to mitochondrial depolarization, mitochondrial ROS production, and activation of the mTOR pathway, all converging to inflammasome activation [22, 29] (Figure 3*A*). To assess the impact of mitochondrial metabolic alterations in IL-1β production by *M. tuberculosis*-infected macrophages, we inhibited succinate dehydrogenase (SDH) with DMM (Figure 3*A*). DMM markedly decreased IL-1β protein in infected BMDM, irrespective of the *M. tuberculosis* clinical isolate (Figure 3*B*), but did not affect *Il1b* transcription (Figure 3*B*). This suggests an effect of DMM in NLRP3 inhibition through the mitochondrial respiratory chain (Figure 3*A*). However, macrophage staining with Mitotracker Red CMXRos revealed no major alterations in mitochondrial membrane potential between the 2 infections (Supplementary Figure 2*A*). Additionally, mitochondrial ROS sequestration with mitoTEMPO (Figure 3*C*) or mTOR blockade with rapamycin (Figure 3*D*) did not impact IL-1β secretion or *Il1b* transcription. None of the mitochondrial inhibitors altered cell viability (Supplementary Figure 2*B*), nor bacteria uptake (Supplementary Figure 2*C*). As a control, mitoTEMPO and rapamycin reduced IL-1β secretion by BMDM stimulated with lipopolysaccharide (LPS) + ATP (Supplementary Figure 2*D* and 2*E*), a condition that induces IL-1β secretion in a mitochondrial ROS-dependent way [29, 30]. Thus, IL-1β secretion by *M. tuberculosis*-infected BMDM may be independent of ETC alterations, unlike what has been reported in single-TLR–based systems [14, 23].

As for BMDM, only inhibition of glycolysis (with 2-DG or in medium without glucose) or of SDH (with DMM) lowered IL-1β secretion in *M. tuberculosis* 4I2-infected mouse alveolar macrophages or bone marrow monocytes, and macrophages differentiated from the human monocytic cell line THP1 (Figure 4*A*–*C*). Consistent with this, a decrease in inflammasome activation was detected in *M. tuberculosis* 4I2-infected THP1-ASC-GFP reporter cells upon glycolysis or SDH inhibition, whereas mitochondrial ROS sequestration and mTOR inhibition resulted in a sustained percentage of ASC-speck–positive cells (Figure 4*D* and Supplementary Figure 3).

Collectively, our findings suggest that canonical pathways linking mitochondrial metabolism and inflammasome activation operate differently upon complex stimuli (live *M. tuberculosis*) when compared to single-TLR stimulation.

M. tuberculosis Clinical Isolates Elicit Similar Metabolomic Profiles in Infected Macrophages

To elucidate why SDH inhibition decreased IL-1β secretion in infected macrophages, we performed an extracellular (cell culture supernatants) and intracellular (cell extracts) NMR metabolomic analysis. This included BMDM cultures (noninfected, infected with *M. tuberculosis* 4I2 or 6C4), and bacterial cultures obtained under the same conditions but without host cells. The baseline levels for different metabolites were defined in medium alone, with deviations above or below representing respectively excretion or consumption.

PCA of the extracellular metabolome (Figure 5*A*) showed infected cells clustering together, suggesting a similar macrophage metabolic reprogramming in both *M. tuberculosis* infections. As above, *M. tuberculosis*-infected BMDM consumed more glucose and secreted more lactate than noninfected macrophages, irrespective of the infecting clinical isolate (Figure 5*B*). This was accompanied by a slight increase in pyruvate consumption and no effect on fructose (Figure 5*B*). Infected BMDM cultures also showed increased itaconate and glutamate release, again with no differences between *M. tuberculosis* isolates (Figure 5*B*). Most of the detected metabolites were similar between the 2 infections and the isolates cultured in the absence of BMDM, and mainly unaffected as compared to the culture medium (Figure 5*B* and Supplementary Figure 4).

The intracellular metabolome PCA plot showed some separation between cellular and bacteria-only conditions (Figure 5*C*). However, infected cells clustered together, supporting that no substantial metabolic differences exist between infections with the 2 clinical isolates. Consistent with the extracellular metabolome data and descriptions for other bacterial infections [31–33], we detected an increase of itaconate and alanine in infected cells (Figure 5*D*). We did not detect an intracellular accumulation of succinate or ATP + ADP upon infection (Figure 5*D*). Other detected metabolites were also similarly modulated, irrespectively of the *M. tuberculosis* isolate (Supplementary Figure 4).

In essence, both infections induced similar macrophage metabolic alterations, including a glycolytic shift and an increase in TCA cycle by-products, which did not include succinate.

IL-1β Production by *M. tuberculosis*-Infected Macrophages Is Independent of HIF-1α and IRG1 Activity

Succinate is linked to the stabilization of HIF-1α, a transcription factor for *Il1b* [21, 34], while itaconate is associated to SDH and NLRP3 inhibition [12, 35] (Figure 6*A*). Thus, we tested the contribution of these pathways to IL-1β production by *M. tuberculosis*-infected macrophages. When compared to wild-type mice, infection of mHIF1α$^{-/-}$ BMDM with either *M. tuberculosis* isolate yielded no effect on IL-1β protein levels,

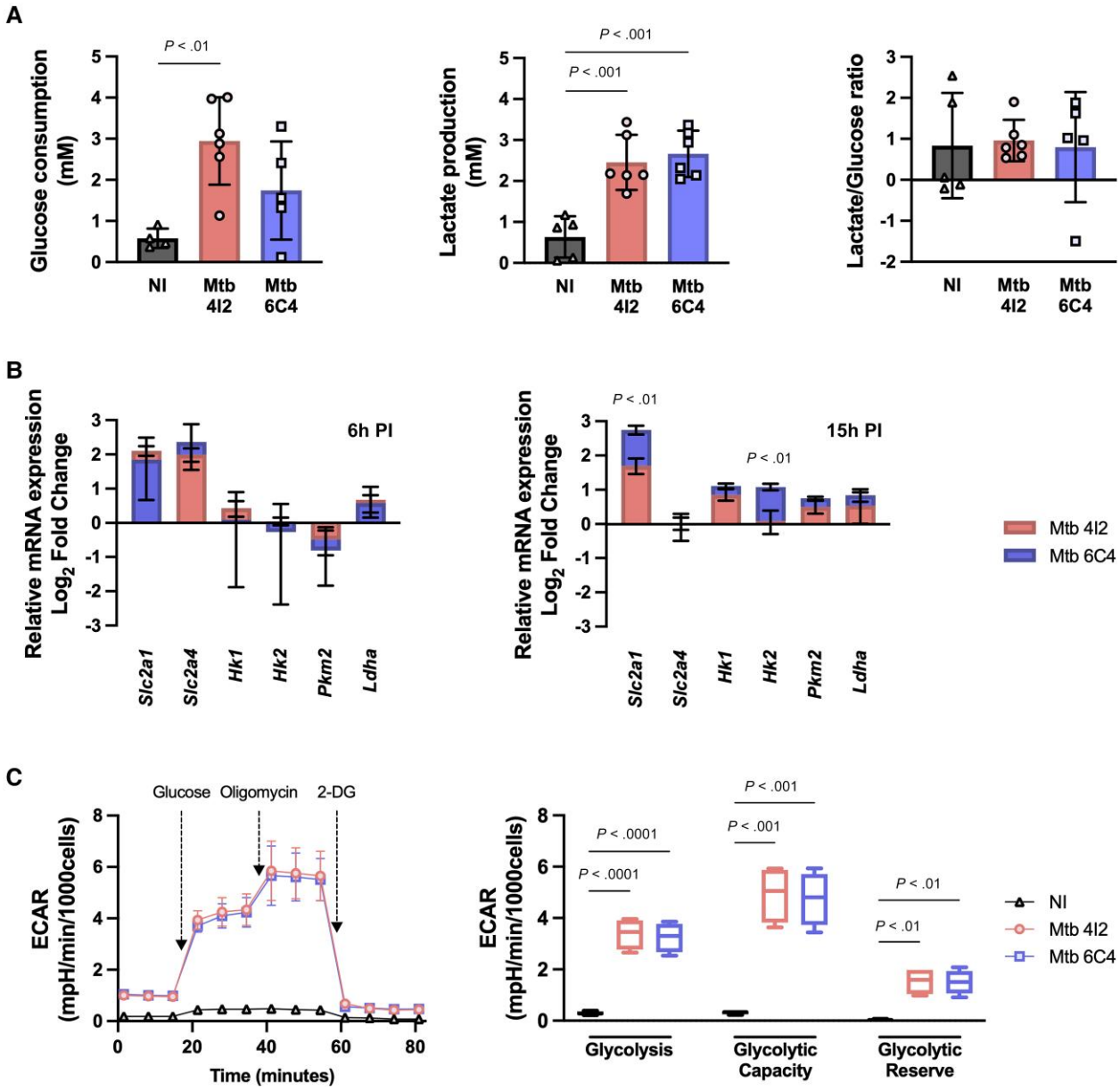

Figure 2. Glycolysis does not differ between the 2 *Mycobacterium tuberculosis* clinical isolates. *A* and *B*, BMDM from C57BL/6 mice were infected at an MOI of 2 with either clinical isolate. *A*, Glucose consumption and lactate production were measured through HPLC in the supernatant of infected cultures after 24 hours, and the lactate/glucose ratio was calculated based on these values. *B*, Six and 15 hours postinfection, cell cultures were lysed and the expression of the indicated genes determined by real-time PCR. Data are represented in $\log_2$ (fold change), with 0 representing noninfected macrophages. *C*, BMDM infected at MOI of 2 for 24 hours were submitted to glycolysis stress test. ECAR was measured with an XFp Analyzer. Glycolysis, glycolytic capacity, and glycolytic reserve were calculated. Represented is the mean ± SD of triplicate (*A* and *B*) or duplicate (*C*) wells for 2 experiments (*A* and *C*) or 1 experiment representative of 2 (*B*). For ECAR assays (*C*) data are also represented in a box and whiskers plot (Tukey method). Statistical analysis was performed using 1-way ANOVA (*A* and *C*) or 2-tailed unpaired Student *t* test (*B*). Abbreviations: 2-DG, 2-deoxy-glucose; BMDM, bone marrow-derived macrophages; ECAR, extracellular acidification rate; HPLC, high-performance liquid chromatography; IL-1β, interleukin 1β; MOI, multiplicity of infection; Mtb, *M. tuberculosis*; NI, noninfected; PI, postinfection.

with only minor differences in *Il1b* mRNA (Figure 6*B*). Similarly, lack of IRG1 [36], the enzyme that converts aconitate into itaconate, showed no impact on IL-1β secretion or *Il1b* transcription (Figure 6*C*). With exception for the effect of DMM, our data show that the TCA cycle and IL-1β production may be uncoupled in certain systems.

DMM Acts on the Pathogen to Inhibit IL-1β Secretion by Infected Macrophages

The effect of DMM on IL-1β was posttranscriptional, not related to the usual host metabolic players, and involved inflammasome inhibition (Figures 3–6), which paralleled the outcome of inhibiting of the bacterial metabolism with rifampicin during

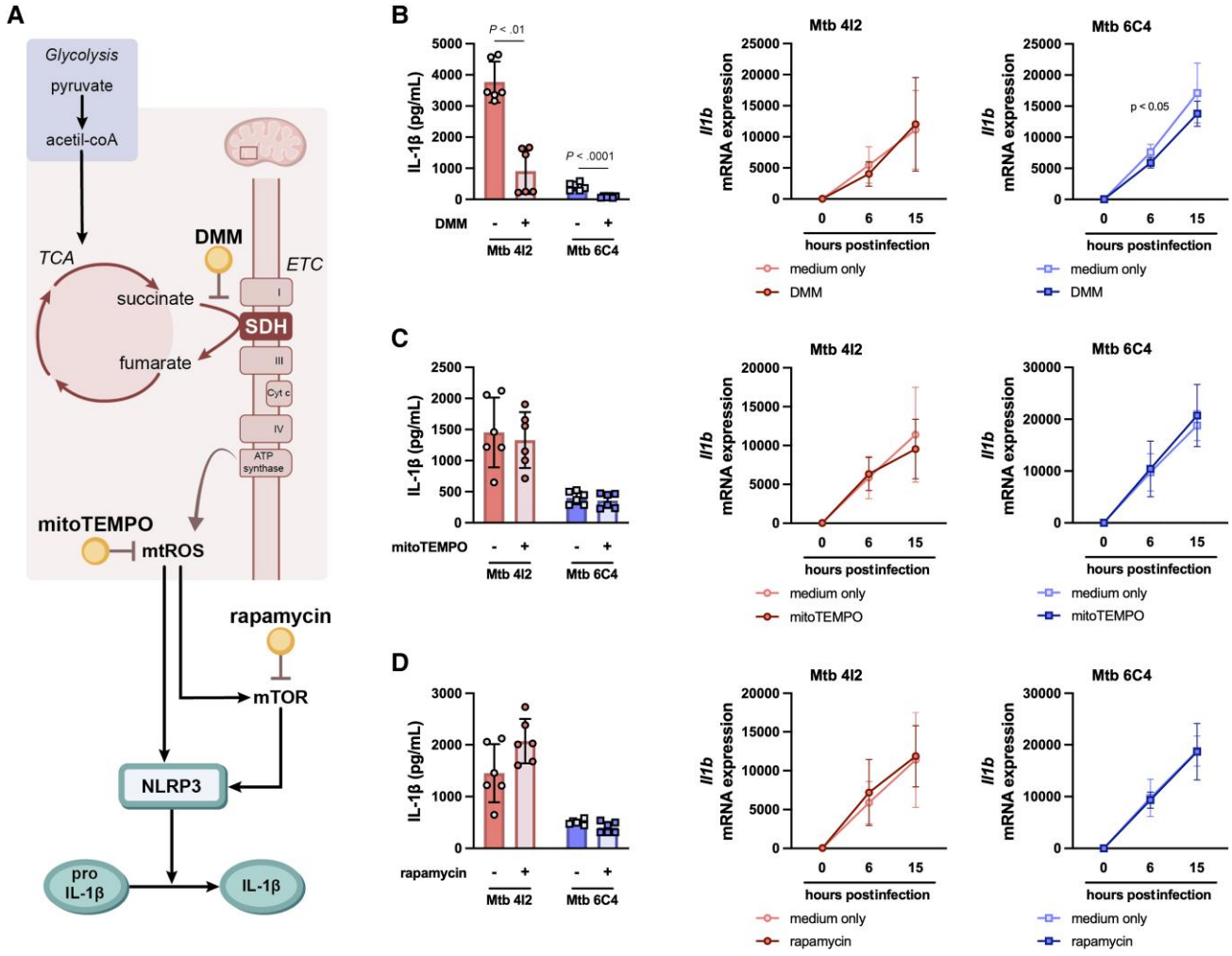

Figure 3. DMM inhibits inflammasome activation and IL-1β production independently of mitochondrial ROS and mTOR. *A*, DMM, mitoTEMPO, and rapamycin inhibitory action within the metabolic pathway. *B–D*, BMDM from C57BL/6 mice were left untreated (–) or pretreated (+) for 2 hours with DMM (*B*), mitoTEMPO (*C*), or rapamycin (*D*) and subsequently infected with either clinical isolate at a multiplicity of infection of 2. The inhibitors were maintained in the cultures throughout the incubation period, with exception of rapamycin which was only present for 2 hours. The amount of secreted IL-1β was quantified in the cell culture supernatants 24 hours postinfection. Six and 15 hours postinfection, cell cultures were lysed and *Il1b* expression measured by real-time PCR. Represented is the mean ± SD of triplicate wells for 2 experiments. Statistical analysis was performed using 2-tailed unpaired Student *t* test. Abbreviations: BMDM, bone marrow-derived macrophages; DMM, dimethyl malonate; ETC, electron transport chain; IL-1β, interleukin 1β; Mtb, *M. tuberculosis*; mTOR, mammalian target of rapamycin; mtROS, mitochondrial reactive oxygen species; SDH, succinate dehydrogenase; TCA, tricarboxylic acid.

infection [20]. So, we hypothesized that DMM might primarily interfere with the bacterial, not the host, metabolism.

M. tuberculosis encodes 3 SDH enzymes: SDH-1 (Rv0247c to Rv0249c), SDH-2 (Rv3316 to Rv3319), and fumarate reductase (Rv1552 to Rv1555) [37, 38]. We focused on SDH-1, which is highly homologous to the *M. smegmatis*-encoded molecule and has a published structure and predicted electron transfer mechanism [39]. The structure of *M. tuberculosis* SDH-1 was predicted using ColabFold [26] and superpositioned with the resolved structure of *M. smegmatis* SDH-1 containing the ligand ubiquinone-1 (instead of menaquinone, PDB: 7D6 V; Figure 7*A*, left). The electron transfer pathway in *M. tuberculosis* SDH-1 is likely similar to that of *M. smegmatis* SDH-1, predicted to occur from succinate oxidation in the flavoprotein domain (shown in cyan; Figure 7*A*, left and middle) to the quinone binding site (in green; Figure 7*A*, left and middle), through redox centers (in yellow; Figure 7*A*, left and middle) [39]. Furthermore, the redox centers arrangement is similar to the mammalian SDH [40], and likely inhibited by the same small molecules, that is DMM. Thus, DMM may bind directly to the SDH quinone-binding domain (Figure 7*A*, middle and right), or be converted into malonate competing for the SDH succinate binding site (Figure 7*A*, middle and right) [41].

To distinguish the impact of DMM on the host versus bacteria, we compared macrophages, pretreated with inhibitors, during infection (affecting the host, and potentially the pathogen)

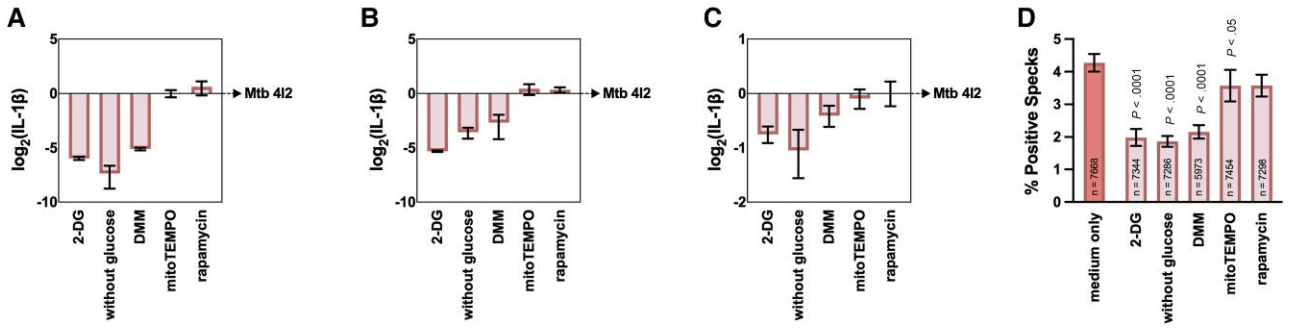

Figure 4. The impact of metabolic inhibitors on IL-1β is not cell specific. *A*, Alveolar macrophages, (*B*) bone-marrow-derived monocytes from C57BL/6 mice, and (*C*) THP1-ASC-GFP macrophages were left untreated (–) or pretreated (+) with the indicated inhibitors for 2 hours and infected with *Mycobacterium tuberculosis* 4I2 at an MOI of 1 for 24 hours. The inhibitors were maintained in the cultures throughout the incubation period, with exception of rapamycin which was only present for 2 hours. The amount of secreted IL-1β was quantified in the cell culture supernatants. Data are represented in $\log_2$ (fold change), with 0 representing macrophages infected with *M. tuberculosis* 4I2. *D*, Phorbol 12-myristate 13-acetate (PMA)-differentiated THP-1-ASC-GFP were treated with inhibitors for 2 hours as indicated in the figure and infected with *M. tuberculosis* 4I2 at an MOI of 1 and the percentage of speck-positive cells determined 6 hours postinfection. Represented is the mean ± SD of triplicate wells for 1 experiment (*A* and *D*) or 2 experiments (*B* and *C*). For immunofluorescence, 60 fields per replicate (total number of cells indicated in each bar) were acquired and analyzed. Statistical analysis was performed using 1-way ANOVA (*D*). Abbreviations: 2-DG, 2-deoxy-glucose; DMM, dimethyl malonate; IL-1β, interleukin 1β; MOI, multiplicity of infection; Mtb, *M. tuberculosis*.

versus pretreating the pathogen with inhibitors and washing it out before infection (targeting mainly the pathogen; Figure 7*B*). As before (Figure 1), BMDM exposure to 2-DG highly impacted IL-1β secretion (Figure 7*B*), whereas pretreating *M. tuberculosis* with 2-DG did not, showing a host-specific effect for 2-DG (Figure 7*B*). In contrast, DMM impacted IL-1β secretion similarly for both experimental conditions (Figure 7*B*) suggesting that affecting the bacteria was enough to decrease IL-1β secretion. The effect of DMM was more pronounced in *M. tuberculosis* 4I2 than in isolate 6C4, fitting in with our previous data for differential inflammasome activation by these *M. tuberculosis* isolates [20]. In turn, Q203, a specific inhibitor of the *M. tuberculosis* respiratory chain [42], only impacted pathogen-mediated IL-1β secretion (Figure 7*B*). Of note, BMDM infected with DMM-treated bacteria showed no differences in *Il1b* transcript when compared to DMM-treated BMDM (Supplementary Figure 5*A*), further supporting its post-transcriptional effect. Lastly, pretreatment of *M. tuberculosis* 4I2 with DMM or Q203 decreased the activation of the host inflammasome measured in THP1-ASC-GFP reporter cells, unlike pretreatment with 2-DG (Figure 7*C* and Supplementary Figure 5*B*).

Collectively, these data suggest that DMM inhibits pathogen metabolism by targeting bacterial SDH. Given the high similarity of SDH across *M. tuberculosis* isolates, DMM is likely effective against all isolates. However, for isolates like 4I2, which require metabolic activity to activate the host inflammasome, DMM subsequently reduces host IL-1β production. In summary (Figure 7*D*), our results position the macrophage glycolytic shift promoted by *M. tuberculosis* infection and the bacterial metabolism as critical for IL-1β production, with no apparent contribution of the host TCA cycle and ETC, contrasting previously described findings for single-TLR agonists.

DISCUSSION

M. tuberculosis diversity significantly impacts host-pathogen interactions and tuberculosis outcomes, with closely related strains employing distinct and highly effective mechanisms to subvert host responses [20, 43–45]. Several studies have shown that *M. tuberculosis* infection shifts macrophage metabolism from oxidative phosphorylation to glycolysis [4, 5, 46, 47], but other investigations report that *M. tuberculosis* infection decelerates or limits the host metabolism [6, 46, 48, 49]. Whether genetically diverse isolates modulate this process remained largely unexplored [6, 7]. Here, we investigated the metabolic adaptation of macrophages to infection with genetically diverse clinical isolates that distinctly modulate NLRP3 activation and IL-1β production in a host-independent manner [20].

We report that despite downstream strain-specific differences in inflammasome activation and IL-1β production, the 2 *M. tuberculosis* clinical isolates elicited similar glycolytic responses in macrophages, indicating a shared bioenergetic profile. This suggests that while bacterial genetic variation affects macrophage cytokine responses, the energetic requirements to mount this initial immune response are conserved. Additionally, our study underpins the glycolytic pathway as a crucial regulator of IL-1β production during *M. tuberculosis* infection, impacting both *Il1b* transcription and NLRP3 activation. We also investigated the interplay between the TCA cycle and inflammasome activation in infected macrophages, as DMM significantly decreased IL-1β production in these cells

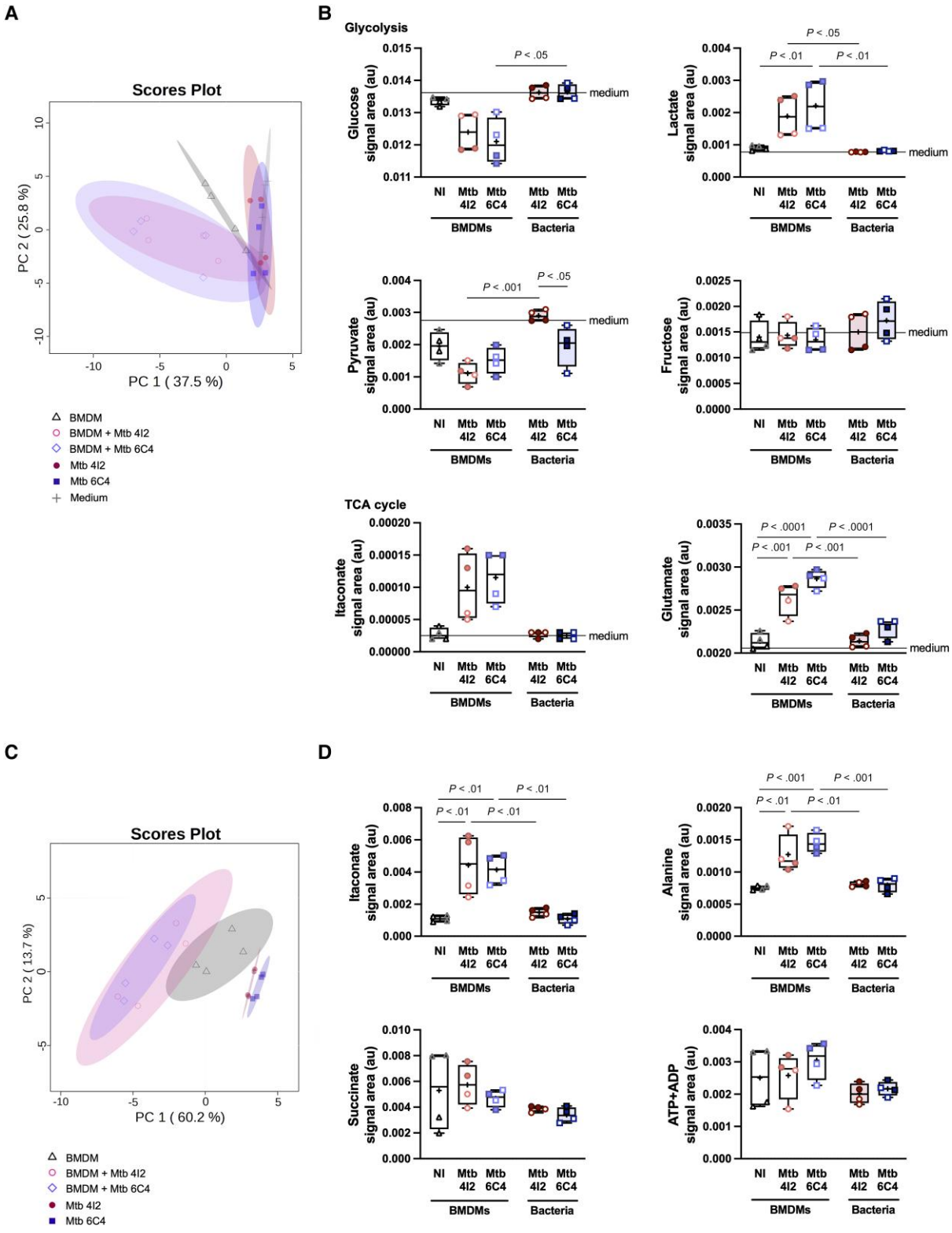

Figure 5. NMR-based metabolomic analysis of macrophages infected with *Mycobacterium tuberculosis* clinical isolate 4I2 or 6C4 reveals similar metabolic profiles. *A*, PCA of spectral data from the culture supernatants of noninfected BMDM, macrophages infected with *M. tuberculosis* 4I2 or 6C4 for 24 hours at a multiplicity of infection of 2, and *M. tuberculosis* 4I2 or 6C4 cultured in similar medium but in the absence of host cells. *B*, Representative metabolites consumed and excreted in the tested conditions. Variations are expressed in relation to media only. *C*, PCA of spectral data recorded for intracellular aqueous extracts in the same conditions as in (*A*). *D*, Relative intracellular levels of representative metabolites across the tested conditions. Represented are box and whisker plots (Tukey method) of duplicate wells for 2 experiments. Each replicate is a pool of 24 wells in a 24-well plate. Statistical analysis was performed using 1-way ANOVA. Abbreviations: au, arbitrary unit; BMDM, bone-marrow derived macrophages; Mtb, *M. tuberculosis*; NI, noninfected; PCA, principal component analysis; TCA, tricarboxylic acid.

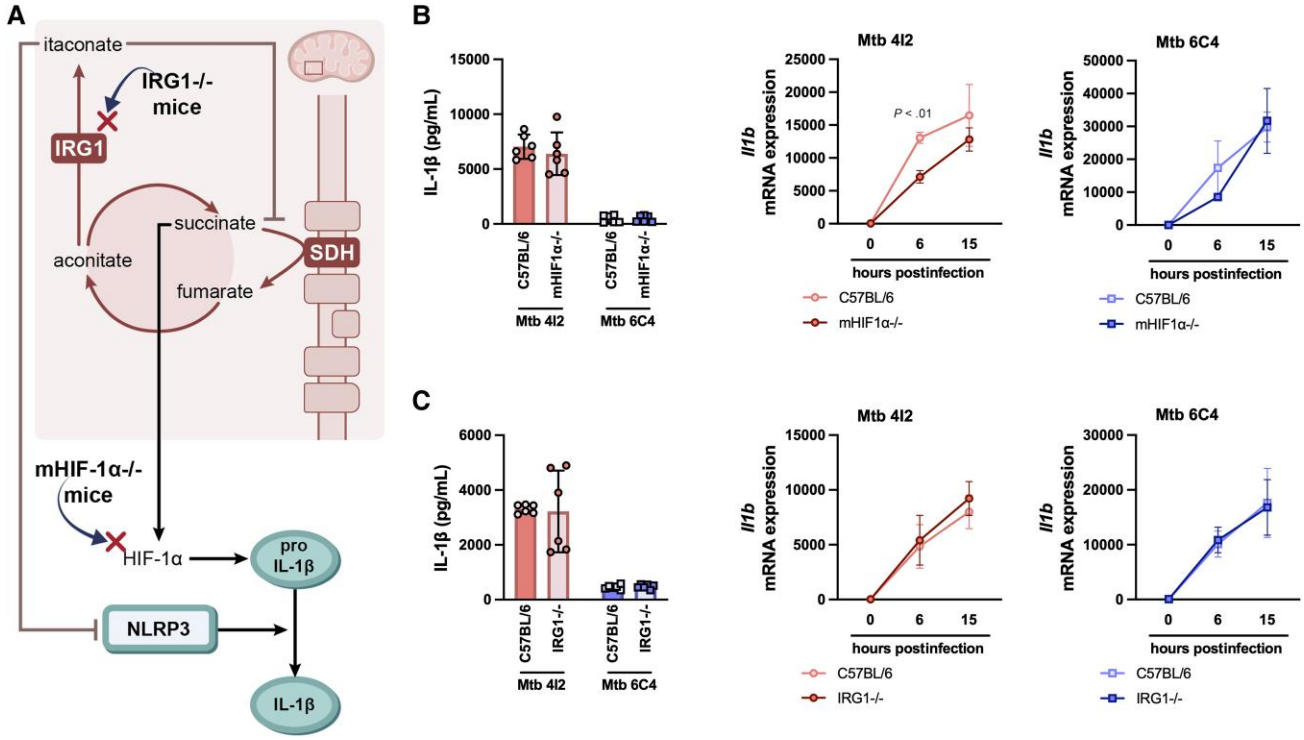

Figure 6. IL-1β production by *Mycobacterium tuberculosis*-infected macrophages is independent of HIF-1α and IRG1 activity. *A*, HIF-1α and IRG1 pathways and their impact on IL-1β regulation. *B* and *C*, BMDM from C57BL/6 and mHIF-1α$^{-/-}$ (*B*) or IRG1$^{-/-}$ (*C*) mice were infected with either clinical isolate at a multiplicity of infection of 2 for 24 hours. The amount of secreted IL-1β was quantified in the cell culture supernatants 24 hours postinfection. Six and 15 hours postinfection, cell cultures were lysed and the *Il1b* expression measured by real-time PCR. Represented is the mean ± SD of triplicate wells for 2 experiments (*B* and *C*) or 1 experiment (*B*) representative of 2. Statistical analysis was performed using a 2-tailed unpaired Student *t* test. Abbreviations: BMDM, bone-marrow derived macrophages; HIF-1α, hypoxia-inducible factor 1 subunit α; IL-1β, interleukin 1β; IRG1, immune responsive gene 1; Mtb, *M. tuberculosis*; PCR, polymerase chain reaction; SDH, succinate dehydrogenase.

due to posttranscriptional modulation. However, surprisingly, mitochondrial ROS sequestration, mTOR inhibition, or HIF-1α deletion did not impact IL-1β secretion. Departing from current immunometabolic models based on single-TLR activation [12, 21, 22], our findings suggest that during macrophage infection with live *M. tuberculosis,* inflammasome activation may be uncoupled from the TCA cycle. Further supporting the hypothesis that canonical pathways conventionally linked to inflammasome activation may operate differently under single (eg, LPS) versus complex stimuli (eg, live *M. tuberculosis*), metabolomic analyses revealed overwhelmingly similar macrophage metabolic profiles in response to both *M. tuberculosis* isolates. Our observations, indicating that the differential activation of the inflammasome and subsequent IL-1β production in macrophages infected with distinct *M. tuberculosis* isolates are not linked to differential metabolic requirements, contradict our original hypothesis. Future investigations should explore alternative molecular mechanisms at play in infected cells. Promising avenues include examining the dynamics of phagolysosome formation or rupture induced by these different isolates, as well as potential alterations in macrophage autophagic flux. These findings open new research perspectives on the immunometabolic control of cytokine responses.

The evidence that DMM inhibited inflammasome activation and IL-1β production without the contribution of common host pathways was puzzling. We hypothesized that DMM may interfere with pathogen metabolism rather than macrophage metabolic adaptation to infection. Combining structural prediction of the *M. tuberculosis* SDH with stimulation of macrophages with *M. tuberculosis* preexposed to DMM, we concluded that this was indeed the case. It remains to be established whether DMM affects mycobacterial replication or the production/abundance of virulence factors (ie, PDIM, PknF, or ESX-1 components) needed for NLRP3 activation. It will be important to further investigate the molecular pathways triggered in the pathogen, as both our previous [20] and current study show that inflammasome activation and high IL-1β induction in infected macrophages depended on the presence of live, metabolically active bacteria.

In conclusion, our study demonstrates that observations from experiments with single bacteria-derived moieties may not be valid in context of live organisms and that during *M. tuberculosis* infection IL-1β production primarily relies on bacteria-specific mechanisms. These findings are critical for in-depth and accurate understanding of the infectious process and

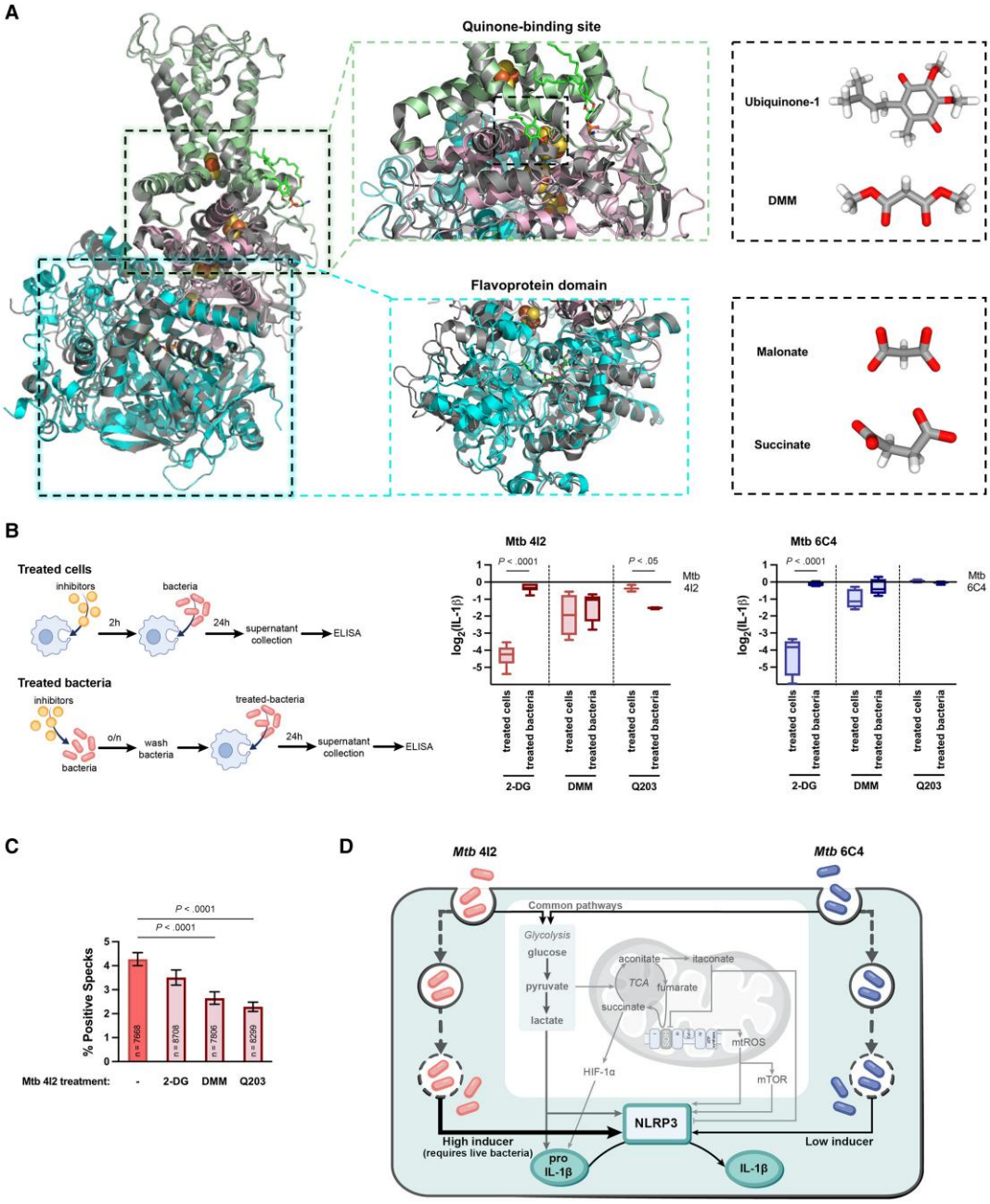

Figure 7. Infection of macrophages with *Mycobacterium tuberculosis* 4I2 exposed to DMM results in reduced inflammasome activation and IL-1β production. *A*, *M. tuberculosis* SDH-1 protein structure predicted with ColabFold. Flavoprotein domain (represented in cyan), iron-sulfur domain (represented in pink), and membrane anchor domain (represented in green) are superpositioned with SDH-1 from *Mycobacterium smegmatis* in complex with ubiquinone-1 (7D6V, grey). Redox centers (represented in yellow/orange) include the flavin-adenine nucleotide (FAD), the [2Fe-2S], [4Fe-4S], [3Fe-4S] iron-sulfur cluster, and the Rieske-type [2Fe-2S] cluster. Ubiquinone-1 (CID 4462), DMM (CID 7943), malonate (CID 9084), and succinate (CID 160419) structures were extracted from PubChem. *B*, Schematic representation of the protocol for treating bacteria or macrophages with metabolic inhibitors. *M. tuberculosis* 4I2 and 6C4 or C57BL/6 BMDM were pretreated with the indicated inhibitors according to the protocol. Treated macrophages were infected with nontreated bacteria and nontreated macrophages were infected with treated bacteria, at an MOI of 2 for 24 hours. The amount of secreted IL-1β was quantified in the cell culture supernatants. Data are represented in $\log_2$ (fold change), with 0 representing nontreated macrophages infected with nontreated *M. tuberculosis* 4I2 or 6C4. *C*, THP1-ASC-GFP macrophages were infected with treated *M. tuberculosis* 4I2, at an MOI of 1 for 6 hours and the percentage of speck-positive cells was determined for the different conditions. Represented are box and whiskers plots (Tukey method) (*B*), or the mean ± SD (*C*) of triplicate wells for 2 experiments (*B*) or 1 experiment (*C*). For immunofluorescence, 60 fields (total number of cells indicated in each bar) per replicate were acquired and analyzed. Statistical analysis was performed using 1-way ANOVA. *D*, Model of the macrophage immunometabolic adaptation during *M. tuberculosis* infection and its interaction with the inflammasome activation and IL-1β secretion. Common pathways triggered in response to *M. tuberculosis* 4I2 or 6C4 are shown in the center. The pathways leading to distinct activation of the NLRP3 inflammasome by these clinical isolates remain unknown. Abbreviations: 2-DG, 2-deoxy-glucose; BMDM, bone-marrow derived macrophages; CID, PubChem compound identification; DMM, dimethyl malonate; ELISA, enzyme-linked immunosorbent assay; HIF-1α, hypoxia-inducible factor 1α; IL-1β, interleukin 1β; MOI, multiplicity of infection; Mtb, *M. tuberculosis*; mTOR, mammalian target of rapamycin; mtROS, mitochondrial reactive oxygen species; o/n, overnight; SDH, succinate dehydrogenase; TCA, tricarboxylic acid.

its metabolic regulation. Furthermore, the impact of host-designed metabolic inhibitors on the pathogen raises awareness of conserved biological pathways and could facilitate the design of new therapies.

Supplementary Data

Supplementary materials are available at *The Journal of Infectious Diseases* online (http://jid.oxfordjournals.org/). Supplementary materials consist of data provided by the author that are published to benefit the reader. The posted materials are not copyedited. The contents of all supplementary data are the sole responsibility of the authors. Questions or messages regarding errors should be addressed to the author.

Notes

Author contributions. A. I. F., I. F. D., R. S., A. D., and M. S. contributed conceptualization. A. I. F., A. J. P., I. F. D., A. D., and M. S. performed formal analysis. I. F. D., R. S., and M. S. acquired funding. A. I. F., A. J. P., D. S., U. Z., C. F., I. F. D., and M. S. performed investigations. M. S. contributed project administration. I. F. D., R. S., A. D., and M. S. contributed resources. R. S., A. D., and M. S. contributed supervision. A. I. F., A. J. P., and M. S. contributed visualization and wrote the draft. All authors contributed writing review and editing.

Acknowledgements. We thank Drs Gil Castro, Tiago Beites, and Joana Couto for critically reading the manuscript. The authors thank the support from the Instituto de Investigação e Inovação em Saúde scientific platforms animal facility, translational cytometry, and biosciences screening, a member of PT-OPENSCREEN (NORTE-01-0145-FEDER-085468), and Portuguese platform of BioImaging (PPBI; PPBI-POCI-01-0145-FEDER-022122).

Financial support. This work was supported by the Portuguese Foundation for Science and Technology (FCT; grant numbers PTDC/SAU-INF/1172/2021 and CEECIND/00241/2017 to M. S., CEECIND/02387/2018 to I. F. D, and 10.54499/2020.00185.CEECIND/CP1600/CT0004 to R. S.). A. I. F. was supported by the FCT (grant number 2020.05949.BD PhD scholarship); the European Federation of Immunological Societies-Immunology Letters (short-term fellowship); and the European Society of Clinical Microbiology and Infectious Diseases (research grant 2022). D. S. was supported by the FCT (grant number SFRH/BD/143536/2019 PhD fellowship). This work was also supported by the project CICECO-Aveiro Institute of Materials UIDB/50011/2020 (DOI 10.54499/UIDB/50011/2020), UIDP/50011/2020 (DOI 10.54499/UIDP/50011/2020) and LA/P/0006/2020 (DOI 10.54499/LA/P/0006/2020), financed by national funds through the FCT/MEC (PIDDAC), and projects 10.54499/UIDB/50026/2020, 10.54499/UIDP/50026/2020 and 10.54499/LA/P/0050/2020. The NMR spectrometer is part of the National NMR Network, partially supported by Infrastructure Project number 022161, cofinanced by *Fundo Europeu de Desenvolvimento Regional* (FEDER) through COMPETE 2020, *Programa Operacional Competitividade e Internacionalização* (POCI), and PORL, and FCT through PIDDAC.

Potential conflicts of interest. All authors: No reported conflicts. All authors have submitted the ICMJE Form for Disclosure of Potential Conflicts of Interest. Conflicts that the editors consider relevant to the content of the manuscript have been disclosed.

References

1. Van den Bossche J, O'Neill LA, Menon D. Macrophage immunometabolism: where are we (going)? Trends Immunol **2017**; 38:395–406.
2. World Health Organization. Global tuberculosis report 2023. https://iris.who.int/. Accessed 1 September 2024.
3. Shi L, Salamon H, Eugenin EA, Pine R, Cooper A, Gennaro ML. Infection with *Mycobacterium tuberculosis* induces the Warburg effect in mouse lungs. Sci Rep **2015**; 5:18176.
4. Gleeson LE, Sheedy FJ, Palsson-McDermott EM, et al. Cutting edge: *Mycobacterium tuberculosis* induces aerobic glycolysis in human alveolar macrophages that is required for control of intracellular bacillary replication. J Immunol **2016**; 196:2444–9.
5. Lachmandas E, Beigier-Bompadre M, Cheng SC, et al. Rewiring cellular metabolism via the AKT/mTOR pathway contributes to host defence against *Mycobacterium tuberculosis* in human and murine cells. Eur J Immunol **2016**; 46:2574–86.
6. Mendonca LE, Pernet E, Khan N, et al. Human alveolar macrophage metabolism is compromised during *Mycobacterium tuberculosis* infection. Front Immunol **2023**; 13:1044592.
7. Kumar R, Singh P, Kolloli A, et al. Immunometabolism of phagocytes during *Mycobacterium tuberculosis* infection. Front Mol Biosci **2019**; 6:105.
8. Huang L, Nazarova EV, Tan S, Liu Y, Russell DG. Growth of *Mycobacterium tuberculosis* in vivo segregates with host macrophage metabolism and ontogeny. J Exp Med **2018**; 215:1135–52.
9. Pisu D, Huang L, Grenier JK, Russell DG. Dual RNA-Seq of Mtb-infected macrophages in vivo reveals ontologically distinct host-pathogen interactions. Cell Rep **2020**; 30: 335–50.e4.
10. Howard NC, Marin ND, Ahmed M, et al. *Mycobacterium tuberculosis* carrying a rifampicin drug resistance mutation reprograms macrophage metabolism through cell wall lipid changes. Nat Microbiol **2018**; 3:1099–108.
11. Mehrotra P, Jamwal SV, Saquib N, et al. Pathogenicity of *Mycobacterium tuberculosis* is expressed by regulating metabolic thresholds of the host macrophage. PLoS Pathog **2014**; 10:e1004265.

12. Hooftman A, Angiari S, Hester S, et al. The immunomodulatory metabolite itaconate modifies NLRP3 and inhibits inflammasome activation. Cell Metab **2020**; 32:468–78.e7.
13. Garaude J, Acín-Pérez R, Martínez-Cano S, et al. Mitochondrial respiratory-chain adaptations in macrophages contribute to antibacterial host defense. Nat Immunol **2016**; 17:1037–45.
14. Billingham LK, Stoolman JS, Vasan K, et al. Mitochondrial electron transport chain is necessary for NLRP3 inflammasome activation. Nat Immunol **2022**; 23:692–704.
15. Silvério D, Gonçalves R, Appelberg R, Saraiva M. Advances on the role and applications of interleukin-1 in tuberculosis. mBio **2021**; 12:e0313421.
16. Rastogi S, Briken V. Interaction of mycobacteria with host cell inflammasomes. Front Immunol **2022**; 13:791136.
17. Rastogi S, Ellinwood S, Augenstreich J, Mayer-Barber KD, Briken V. *Mycobacterium tuberculosis* inhibits the NLRP3 inflammasome activation via its phosphokinase PknF. PLoS Pathog **2021**; 17:e1009712.
18. Madan-Lala R, Peixoto KV, Re F, Rengarajan J. *Mycobacterium tuberculosis* hip1 dampens macrophage proinflammatory responses by limiting toll-like receptor 2 activation. Infect Immun **2011**; 79:4828–38.
19. Danelishvili L, Everman JL, McNamara MJ, Bermudez LE. Inhibition of the plasma-membrane-associated serine protease cathepsin G by *Mycobacterium tuberculosis* Rv3364c suppresses caspase-1 and pyroptosis in macrophages. Front Microbiol **2012**; 2:281.
20. Sousa J, Cá B, Maceiras AR, et al. *Mycobacterium tuberculosis* associated with severe tuberculosis evades cytosolic surveillance systems and modulates IL-1β production. Nat Commun **2020**; 11:1949.
21. Tannahill GM, Curtis AM, Adamik J, et al. Succinate is an inflammatory signal that induces IL-1β through HIF-1α. Nature **2013**; 496:238–42.
22. Mills EL, Kelly B, Logan A, et al. Succinate dehydrogenase supports metabolic repurposing of mitochondria to drive inflammatory macrophages. Cell **2016**; 167: 457–70.e13.
23. Zotta A, O'Neill LAJ, Yin M. Unlocking potential: the role of the electron transport chain in immunometabolism. Trends Immunol **2024**; 45:259–73.
24. Carrola J, Bastos V, Jarak I, et al. Metabolomics of silver nanoparticles toxicity in HaCaT cells: structure–activity relationships and role of ionic silver and oxidative stress. Nanotoxicology **2016**; 10:1105–17.
25. Wishart DS, Feunang YD, Marcu A, et al. HMDB 4.0: the human metabolome database for 2018. Nucleic Acids Res **2018**; 46:D608–17.
26. Mirdita M, Schütze K, Moriwaki Y, Heo L, Ovchinnikov S, Steinegger M. ColabFold: making protein folding accessible to all. Nat Methods **2022**; 19:679–82.
27. Rosenberg G, Yehezkel D, Hoffman D, et al. Host succinate is an activation signal for *Salmonella* virulence during intracellular infection. Science **2021**; 371:400–5.
28. Riquelme SA, Prince A. Airway immunometabolites fuel *Pseudomonas aeruginosa* infection. Respir Res **2020**; 21: 326.
29. Li X, Zhang X, Pan Y, et al. mTOR regulates NLRP3 inflammasome activation via reactive oxygen species in murine lupus. Acta Biochim Biophys Sin (Shanghai) **2018**; 50: 888–96.
30. Wu KKL, Long KK, Lin H, et al. The APPL1-rab5 axis restricts NLRP3 inflammasome activation through early endosomal-dependent mitophagy in macrophages. Nat Commun **2021**; 12:6637.
31. Schuster EM, Epple MW, Glaser KM, et al. TFEB induces mitochondrial itaconate synthesis to suppress bacterial growth in macrophages. Nat Metab **2022**; 4: 856–66.
32. Jiang Q, Qiu Y, Kurland IJ, et al. Glutamine is required for M1-like polarization of macrophages in response to *Mycobacterium tuberculosis* infection. mBio **2022**; 13: e0127422.
33. Borah K, Beyß M, Theorell A, et al. Intracellular *Mycobacterium tuberculosis* exploits multiple host nitrogen sources during growth in human macrophages. Cell Rep **2019**; 29:3580–91.e4.
34. Jiang M, Chen Z, Li H, et al. Succinate and inosine coordinate innate immune response to bacterial infection. PLoS Pathog **2022**; 18:e1010796.
35. Lampropoulou V, Sergushichev A, Bambouskova M, et al. Itaconate links inhibition of succinate dehydrogenase with macrophage metabolic remodeling and regulation of inflammation. Cell Metab **2016**; 24:158–66.
36. Price JV, Russo D, Ji DX, et al. IRG1 and inducible nitric oxide synthase act redundantly with other interferon-gamma-induced factors to restrict intracellular replication of *Legionella pneumophila*. mBio **2019**; 10: e02629-19.
37. Hartman T, Weinrick B, Vilchèze C, et al. Succinate dehydrogenase is the regulator of respiration in *Mycobacterium tuberculosis*. PLoS Pathog **2014**; 10:e1004510.
38. Cook GM, Hards K, Vilchèze C, Hartman T, Berney M. Energetics of respiration and oxidative phosphorylation in mycobacteria. Microbiol Spectr **2014**; 2:10.1128/microbiolspec.MGM2-0015-2013.
39. Zhou X, Gao Y, Wang W, et al. Architecture of the mycobacterial succinate dehydrogenase with a membrane-embedded Rieske FeS cluster. Proc Natl Acad Sci U S A **2021**; 118:e2022308118.
40. Sun F, Huo X, Zhai Y, et al. Crystal structure of mitochondrial respiratory membrane protein complex II. Cell **2005**; 121:1043–57.

41. Dervartanian DV, Veeger C. Studies on succinate dehydrogenase I. Spectral properties of the purified enzyme and formation of enzyme-competitive inhibitor complexes. Biochim Biophys Acta **1964**; 92:233–47.
42. Hasenoehrl EJ, Wiggins TJ, Berney M. Bioenergetic inhibitors: antibiotic efficacy and mechanisms of action in *Mycobacterium tuberculosis*. Front Cell Infect Microbiol **2021**; 10:611683.
43. Tientcheu LD, Koch A, Ndengane M, Andoseh G, Kampmann B, Wilkinson RJ. Immunological consequences of strain variation within the *Mycobacterium tuberculosis* complex. Eur J Immunol **2017**; 47:432–45.
44. Peters JS, Ismail N, Dippenaar A, et al. Genetic diversity in *Mycobacterium tuberculosis* clinical isolates and resulting outcomes of tuberculosis infection and disease. Annu Rev Genet **2020**; 54:511–37.
45. Carmona J, Cruz A, Moreira-Teixeira L, et al. *Mycobacterium tuberculosis* strains are differentially recognized by TLRs with an impact on the immune response. PLoS One **2013**; 8:e67277.
46. Cumming BM, Addicott KW, Adamson JH, Steyn AJ. *Mycobacterium tuberculosis* induces decelerated bioenergetic metabolism in human macrophages. Elife **2018**; 7: e30169.
47. Vrieling F, Kostidis S, Spaink HP, et al. Analyzing the impact of *Mycobacterium tuberculosis* infection on primary human macrophages by combined exploratory and targeted metabolomics. Sci Rep **2020**; 10:7085.
48. Pacl HT, Chinta KC, Reddy VP, et al. NAD(H) homeostasis underlies host protection mediated by glycolytic myeloid cells in tuberculosis. Nat Commun **2023**; 14: 5472.
49. Hackett EE, Charles-Messance H, O'Leary SM, et al. *Mycobacterium tuberculosis* limits host glycolysis and IL-1β by restriction of PFK-M via microRNA-21. Cell Rep **2020**; 30:124–36.e4.

Rukobia▼
(fostemsavir)

* In associazione con altri antiretrovirali, per i pazienti adulti con infezione da HIV-1 resistente a molti farmaci, per i quali non è altrimenti possibile stabilire un regime antivirale soppressivo[1]

HIV-1 MDR: Virus HIV-1 multiresistente; PLHIV: Persone che vivono con l'HIV.

Classe di rimborsabilità: H
Prezzo al pubblico: (IVA inclusa) al netto degli sconti obbligatori di legge: € 4.951,24
600 mg - compressa a rilascio prolungato - uso orale - flacone (HDPE)
A.I.C. n. 049362015/E (in base 10) (confezione da 60 compresse)
Regime di dispensazione: medicinale soggetto a prescrizione medica limitativa, da rinnovare volta per volta, vendibile al pubblico su prescrizione di centri ospedalieri o di specialisti - infettivologo (RNRL).

La segnalazione delle reazioni avverse sospette che si verificano dopo l'autorizzazione del medicinale è importante, in quanto permette un monitoraggio continuo del rapporto beneficio/rischio del medicinale.

Agli operatori sanitari è richiesto di segnalare qualsiasi reazione avversa sospetta tramite il sito web dell'Agenzia Italiana del Farmaco:
https://www.aifa.gov.it/content/segnalazioni-reazioni-avverse

▼Medicinale sottoposto a monitoraggio addizionale. Ciò permetterà la rapida identificazione di nuove informazioni sulla sicurezza. Agli operatori sanitari è richiesto di segnalare qualsiasi reazione avversa sospetta.

1. Rukobia Riassunto delle Caratteristiche del Prodotto
RCP RUKOBIA

ViiV Healthcare

Codice deposito aziendale: PM-IT-FST-JRNA-250001.
Materiale promozionale rivolto esclusivamente ai medici
Depositato in AIFA il: 15/07/2025.
VIETATA LA DISTRIBUZIONE AL PUBBLICO.

Consulta il Riassunto delle Caratteristiche del Prodotto attraverso il QRcode